Enhanced Mid-Holocene Vegetation Growth and Its Biophysical Feedbacks in China

Weizhe Chen, Zhongshi Zhang, Philippe Ciais, Liangcheng Tan, David Kemp, Nicolas Viovy

Geophysical Research Letters

RESEARCH LETTER
10.1029/2023GL104702

Enhanced Mid-Holocene Vegetation Growth and Its Biophysical Feedbacks in China

Weizhe Chen[1], Zhongshi Zhang[2], Philippe Ciais[3], Liangcheng Tan[4,5], David B. Kemp[1], and Nicolas Viovy[3]

[1]School of Earth Sciences, Hubei Key Laboratory of Critical Zone Evolution, China University of Geosciences, Wuhan, China, [2]Department of Atmospheric Science, School of Environmental Studies, China University of Geosciences, Wuhan, China, [3]Laboratoire des Sciences du Climat et de l'Environnement, LSCE/IPSL, CEA-CNRS-UVSQ, Université Paris-Saclay, Gif-sur-Yvette, France, [4]State Key Laboratory of Loess and Quaternary Geology, Institute of Earth Environment, Chinese Academy of Sciences, Xi'an, China, [5]Institute of Global Environmental Change, Xi'an Jiaotong University, Xi'an, China

Key Points:

- Our work provides a reliable and spatially continuous mid-Holocene vegetation map for China at a resolution of 0.5°
- Calculated mid-Holocene vegetation gross primary productivity of ~7.5 PgC/yr in China is higher than the present day
- Vegetation dynamics should be considered in simulating mid-Holocene terrestrial carbon cycle and climate change for China

Supporting Information:

Supporting Information may be found in the online version of this article.

Correspondence to:

W. Chen,
wzchen@cug.edu.cn

Citation:

Chen, W., Zhang, Z., Ciais, P., Tan, L., Kemp, D. B., & Viovy, N. (2023). Enhanced mid-Holocene vegetation growth and its biophysical feedbacks in China. *Geophysical Research Letters*, *50*, e2023GL104702. https://doi.org/10.1029/2023GL104702

Received 6 JUN 2023
Accepted 4 OCT 2023

Abstract Proxy-based reconstructions show that the climate during the mid-Holocene (MH) was warmer and wetter than the present day in most regions of China, characterized by a northwestward extension of the East Asian summer monsoon and an increase in woody cover. However, climate simulations that neglect vegetation shifts yield cooler climates than proxy-based reconstructions for the MH. Here, we simulate MH vegetation cover, productivity, and terrestrial parameters in China using a state-of-the-art land surface model forced with realistic proxy-based climate data. Our simulations corroborate MH vegetation cover inferred from 246 pollen sites, and indicate a higher vegetation productivity in China, despite the lower CO_2 concentration during the MH compared to the present day. Enhanced vegetation growth during the MH could have affected land surface energy and hydrological budgets through biophysical feedbacks. Our findings highlight the impact of vegetation dynamics on the terrestrial carbon cycle and regional climate in China.

Plain Language Summary Multiple paleoclimate archives illustrate warmer and wetter climate during the mid-Holocene (MH; ~6,000 years ago) than at present in most regions of China. However, current model results and proxy-based reconstructions have some key discrepancies in climate reconstructions, possibly because these climate simulations have overlooked vegetation changes. Therefore, it is essential to develop a vegetation cover map for China to examine the vegetation-climate feedback during the MH. Here, we present reconstructions of mid-Holocene vegetation cover, productivity and terrestrial parameters in China at a very high resolution using a land surface model. Simulation results can reproduce MH vegetation cover indicated by paleo-records and suggest increased tree cover and vegetation productivity in China. Vegetation changes during the MH likely had an important impact on regional climate in China through altering terrestrial parameters. In contrast, multiple-model ensembles in the latest Paleoclimate Modeling Intercomparison Project significantly underestimated MH vegetation growth primarily because of inherent bias in prescribed vegetation maps. This work reveals the critical impact of MH vegetation cover on terrestrial carbon, energy and hydrological budgets in China, and underlines the need to incorporate vegetation dynamics in terrestrial or climate simulations for the past and future.

1. Introduction

During the mid-Holocene (MH, ~6 ka), increased summer insolation and a series of feedbacks caused the East Asian summer monsoon (EASM) to intensify and extend further north relative to the present day (Goldsmith et al., 2017; Piao et al., 2020; Wu et al., 2021). Over the past 22 Kyr, the summer temperature and precipitation likely reached peaks in the early and mid-Holocene (Shi et al., 2021). The MH climate, particularly in summer, was warmer and wetter than the pre-industrial period (PI) in most regions of China (Dong et al., 2022; Yang et al., 2021; Zhou et al., 2021). The average annual precipitation in China during the MH was ~240 mm/yr higher than in the PI period (Chen, Xiao, et al., 2022; Lin et al., 2019). The warm and wet MH climate caused an expansion of tree cover (Gao et al., 2022; Zhang et al., 2021). The broad-leaved mixed and temperate deciduous forest shifted northward by 4–5°, relative to today (Li et al., 2019). Although previous studies have depicted the temporal evolution of vegetation types regionally since the MH, these studies paid less attention to the response of vegetation patterns and land surface parameters (e.g., vegetation productivity and leaf area) to the climate change in China.

The temperature evolution since the MH in China is still under debate owing to an apparent model-data discrepancy (Jiang et al., 2012; Lin et al., 2019). Many paleo-records (e.g., pollen and mollusk) have demonstrated that the summer, winter, or mean annual temperature in East Asia and other Northern Hemisphere regions was higher during the MH than the PI (Dong et al., 2022; Zhang et al., 2022). On the contrary, some modeling and proxy studies have suggested a cooler climate in the MH, both globally (Bova et al., 2021; Liu et al., 2014; Osman et al., 2021), and regionally in China (Jiang et al., 2012). To address this debate, recent modeling studies have investigated additional climate forcings and feedbacks on the warmth during the MH climate (Kaufman & Broadman, 2023). Sensitivity tests have suggested that shifting vegetation distribution led to the MH temperature maximum over the Northern Hemisphere (Thompson et al., 2022). Although these attempts successfully revealed the vegetation feedback on climate warming, they artificially prescribed the vegetation cover across the MH, especially in China. Some of these prescribed vegetation covers were idealized and included many uncertainties.

Land surface models (LSM), incorporated with a dynamic vegetation module (DVM), have advantages in dynamically simulating vegetation distributions, and terrestrial biogeophysical and biogeochemistry processes (Blyth et al., 2021; Krinner et al., 2005). However, previous simulations of the MH vegetation productivity for China often neglected the bias of climate forcing derived from Earth system models (Brierley et al., 2020; He et al., 2005). Recently, based on proxy data and multiple interpolation methods, Chen, Xiao, et al. (2022) built a high-resolution MH temperature and precipitation gridded data set in China, which provides an opportunity to better simulate vegetation. Here, we use a state-of-the-art land surface model and our proxy-based climate fields to simulate vegetation cover, productivity, and terrestrial parameters during the MH in China. Then, we compared our improved gross primary productivity (GPP) estimates with those latest MH simulations derived from the Paleoclimate Modeling Intercomparison Project 4 (PMIP4)/Coupled Model Intercomparison Project Phase 6 (CMIP6) and examined the causes of discrepancies. Finally, the potential climate feedback of vegetation cover changes is assessed.

2. Materials and Methods

2.1. Data Collection and Experimental Design

Meteorological data are required to force the land surface model. The historical climate data came from the CRU-NCEP v8 data set (1901–2016) (Wei et al., 2014). The period between 1901 and 1910 was used as a pre-industrial reference, assuming PI climate was similar to recent climate, as is common practice (Chen et al., 2020; Martin Calvo & Prentice, 2015). The climate forcings for the MH came from two sources. The first is the IPSL-CM6A-LR simulation (Boucher et al., 2020; Braconnot et al., 2021) for the PMIP4 mid-Holocene experiment ("GCM forcing" hereafter). However, the GCM simulations are shown to underestimate the magnitude of MH temperature and precipitation change in most regions of China (Figure S1 in Supporting Information S1). Therefore, the second source is the high-resolution temperature and precipitation gridded data for the MH, which were upscaled from 159 proxy-based reconstructions across China ("UPS forcing" hereafter) (Figure S1 in Supporting Information S1) and well-validated (Chen, Xiao, et al., 2022). These climate data were processed with a bias-correction method (O'ishi & Abe-Ouchi, 2013) to improve the temporal resolution and accuracy for the LSM.

The process-based LSM used in this study is the latest ORCHIDEE-MICT v8.8.0 (ORganizing Carbon and Hydrology in Dynamic EcosystEms) that simulates carbon, water and energy exchanges between the atmosphere and biosphere. The ORCHIDEE-MICT includes a DVM, which simulates vegetation distribution and mainly follows Krinner et al. (2005). The ORCHIDEE-MICT model has been extensively evaluated against present observed carbon and hydrological fluxes (Guimberteau et al., 2018) and has been widely applied in paleoecological studies (Chen et al., 2020; Zhu et al., 2018). We first performed a transient historical simulation from 1901 to 2016, and validated the result with the observed GPP of Yao et al. (2018) for 1982–2015 and the simulated GPP from the TRENDY project for 1860–2016 (Table S1 in Supporting Information S1) (Le Quéré et al., 2018). Then, we carried out two PI simulations, either with prescribed PI vegetation (PIV) for realistic GPP or with DVM activated for natural vegetation distribution. Finally, to examine the importance of vegetation cover and climate forcing on simulated GPP and terrestrial parameters, four MH simulations were performed with either PIV or DVM, and with either GCM or UPS climate forcings (all simulation details are provided in Table S2 in Supporting Information S1). To compare our results with previous GPP simulations for the MH and PI periods, we collected GPP from nine models from the CMIP6/PMIP4 repository (Table S3 in Supporting Information S1) (Otto-Bliesner et al., 2017).

2.2. Biome Evaluation Metrics

To evaluate the vegetation cover simulated by the DVM of the model, a total of 479 and 246 independent sites of pollen-inferred mega-biomes were collected for 0 and 6 ka in China, respectively (Harrison, 2017; Lin et al., 2019). The DVM simulates vegetation distribution at each grid-cell with a maximum of 11 natural plant functional types (PFTs) (Table S4; Text S1 in Supporting Information S1). Thus, to evaluate the simulated vegetation types, the modeling results and pollen-based vegetation reconstructions must be converted into a comparable mega-biome. This process is called biomisation. In this work, we considered a classic PFT-based biomisation approach (Prentice et al., 2011) and a recently proposed biomisation approach relying on foliage projective cover (FPC-based) (Dallmeyer et al., 2019). The biomisation processes are detailed in Figure S2 in Supporting Information S1.

The best neighbor score (BNS) proposed by Dallmeyer et al. (2019) was adopted to quantify the agreement between our simulations and the pollen-based biome reconstructions. For each pollen site, we first search the corresponding biome type in the simulation result, and then locate the nearest grid (i.e., best neighbor). The BNS for each pollen record (i.e., w) is calculated from the distance between the best neighbor and the pollen location, as follows:

$$w = e^{\frac{-1}{2}\times\left(\frac{\text{distance}}{3}\right)^2} \text{ with distance} = \sqrt{d\text{long}^2 + d\text{lat}^2} \tag{1}$$

Accordingly, w of 0.8 and 0.9 indicate distances of 2° and 1.4°, respectively. The BNS is the mean of all individual calculated w. Because the BNS is derived from records and reduced significantly if different pollen biome types coexist in the same grid, another metric of total accuracy (ACC) is proposed derived from the simulation results. For this metric, we first choose grids where pollen exists in the surrounding 0.5° and then examine whether each grid could be validated by its surrounding pollen records. The ACC is the percentage of validated grids among these examined grids.

3. Results

3.1. Model Performance in Simulating Vegetation Cover and Productivity in China

The performance of the model to simulate natural vegetation types and productivity is quantitatively compared against pollen assemblages and historical observations. Two biomisation methods and two metrics were used to make a quantitative evaluation of the simulated vegetation cover. The BNS for PI and MH DVM simulations are higher than 0.8, indicating a distance of less than 2° on average between pollen sites and the best neighbor in the simulation (Figure 1). ∼60% and ∼75% sites have a BNS higher than 0.95 (i.e., a distance less than 1°) for the PI and the MH simulations, respectively (Figure S3 in Supporting Information S1). According to the evaluation criterion proposed by Dallmeyer et al. (2019), a BNS of 0.5–0.8 or above 0.8 represents a good agreement or a best agreement, respectively. In addition, the ACC values are all higher than 0.9 (Figure 1). Therefore, these metrics suggest that our simulations have a very good agreement with paleo-archives and can capture the natural vegetation patterns. When comparing PI vegetation map (instead of our MH simulation) to MH pollen records, the agreements (i.e., ACC and BNS values) all decrease by ∼0.1 reaching ∼0.8 (Figure S4 in Supporting Information S1). Major discrepancies are found in marginal monsoon regions and regions with intense anthropogenic land use. This mismatch implies it is inaccurate to substitute MH vegetation with prescribed PI vegetation in PMIP4 MH simulations for China.

According to a recent observation-based estimate, the mean annual GPP over China was ∼6.6 PgC/yr during 1982–2015 (Yao et al., 2018). Compared to this value, GPP results from TRENDY multiple models overestimate the GPP in China by 15% ± 5%. Our historical simulation (with a slight overestimation by 8%) is at the lower end of the TRENDY 10%–90% percentile range and is more comparable to the observation-based estimate (Figure 2c). This slight overestimate is mostly attributable to modern human activities (Anav et al., 2015), which disturb many ecosystems and reduce vegetation cover and growth. Similarly, in our MH and PI simulations, the estimated GPP with prescribed PI vegetation is at the lower end of PMIP4 and CMIP6 ensembles, respectively, indicating that previous simulations may systematically overestimate GPP in China. The historical simulation is further evaluated against observed net primary productivity (NPP) and leaf area index (LAI) data, because NPP determines vegetation competition in the model and LAI affects the vegetation biophysical feedbacks. The

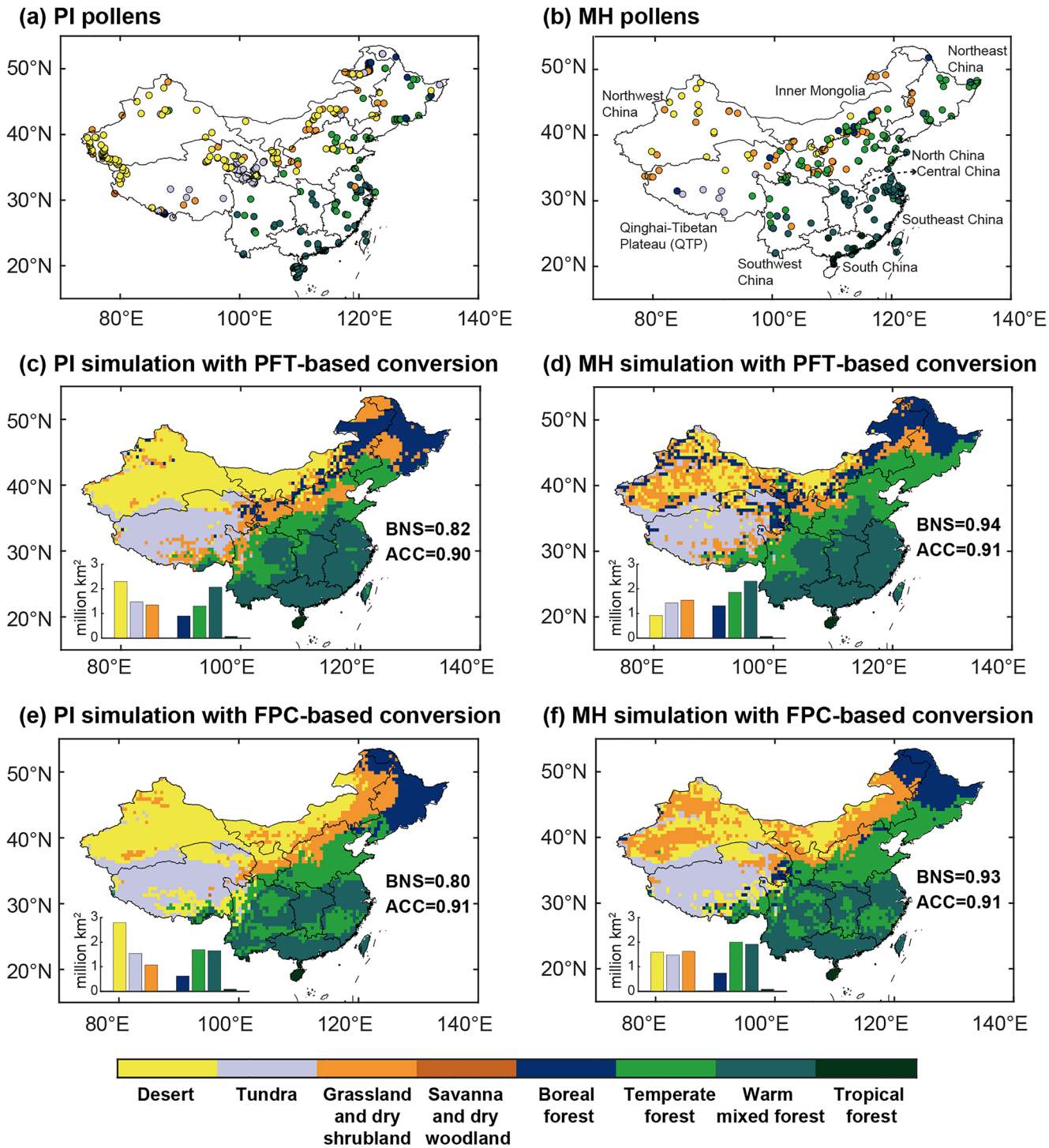

Figure 1. Comparison of mega-biomes in China for the pre-industrial (PI, left column) and mid-Holocene periods (MH, right column). (a–b) Pollen-based biome reconstructions (Harrison, 2017; Lin et al., 2019). Vegetation distributions in PI_DVM and MH_UPS_DVM simulations with PFT-based conversion (c–d) and FPC-based conversion (e–f), respectively. The best neighbor score (BNS) and total accuracy (ACC) are two metrics representing the agreement of the reconstructed biomes and the simulated biome distributions. The inset bar graphs show areas of each mega-biome.

comparison shows a good agreement for the two variables between our simulation and observations (Figure S5 in Supporting Information S1). Taken together, these evaluations suggest that the model is able to correctly reproduce vegetation cover and productivity in China.

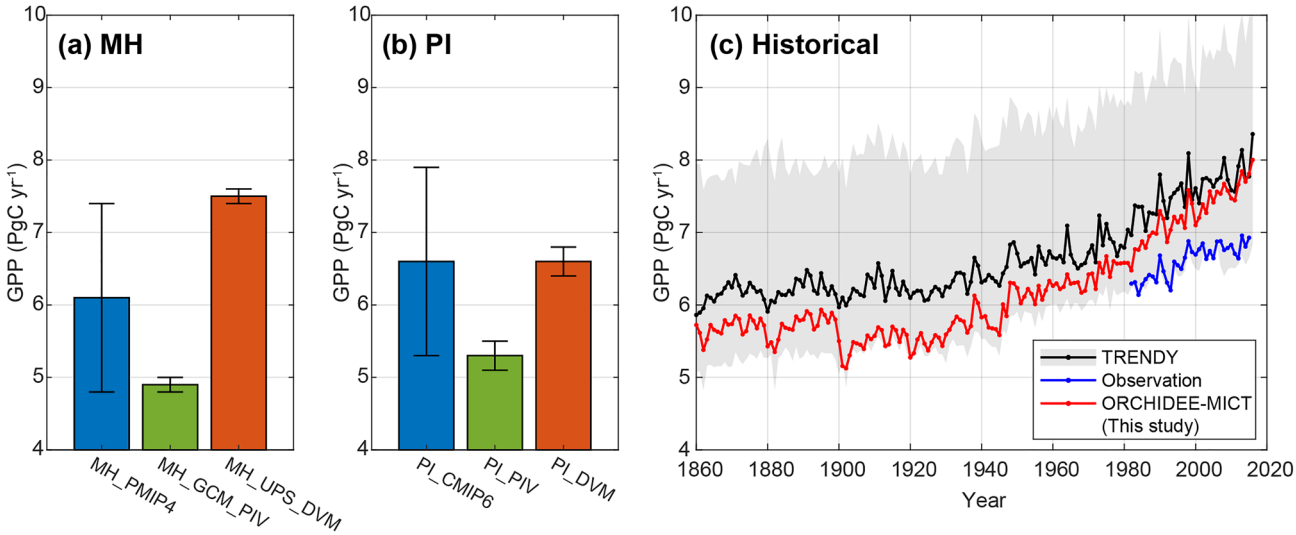

Figure 2. Gross primary productivity (GPP) in China during the mid-Holocene (MH), pre-industrial (PI) and historical periods. (a–b) MH_PMIP4 and PI_CMIP6 (blue bars) are from recent model intercomparison project simulations (Otto-Bliesner et al., 2017). Green and red bars show simulations in this study with either prescribed PI vegetation (PIV) or dynamic vegetation model (DVM). GCM and UPS represent climate forcing derived from a general circulation model and upscaled climate data, respectively (see main text for details). The bars show the average GPP of multiple models/years and the standard deviation. (c) Yearly GPP variations in TRENDY models (Le Quéré et al., 2018), this study for 1860–2016 and observation-based GPP from Yao et al. (2018) for 1982–2015. The gray shading shows the 10%–90% percentile range of the model spread in TRENDY.

3.2. Changes in Vegetation Cover and Productivity

The compiled pollen data sets display key differences in biome distributions between the MH and the PI (Figures 1a and 1b). In the MH, forests existed where grassland and desert appeared in PI, for example, North China and Inner Mongolia; grassland occurred in Northwest China, where desert formed in the PI. Consistent with the pollen data sets, the simulated desert area is largely reduced in the MH_UPS_DVM experiment (~1.3 million km^2) relative to the PI_DVM experiment (~2.5 million km^2) (Figures 1c–1f). The areas of simulated grassland, and boreal and temperate forest areas in northern China were ~0.4, ~0.3, and ~0.4 million km^2 larger in the MH than the PI, respectively. In addition to vegetation types, the simulated GPP in China is much higher in the MH_UPS_DVM (~7.5 PgC/yr) than in the PI_PIV experiment (~5.3 PgC/yr) (Figure 2). Spatially, the GPP in the MH is higher in North China and Northeast China, benefiting from the warmer and wetter climate (Figure 3e and Figure S1 in Supporting Information S1). Moreover, the simulated MH GPP even exceeds the modern value of ~6.6 PgC/yr (as determined over the past three decades), despite the CO_2 concentration being ~100 ppmv lower during the MH (i.e., ~265 ppmv for 6 ka compared to ~367 ppmv averaged over 1982–2015). This suggests that the beneficial factors of MH wetter and warmer climate in China have offset the negative effect of lower CO_2 concentration and resulted in forest expansion and enhanced vegetation growth.

4. Discussion

4.1. Importance of Vegetation Cover on GPP Reconstructions

Pollen-based studies indicate wide woody encroachment during the MH, for example, in Northeast China (Gao et al., 2022), along the southeastern and eastern margins of the Tibetan Plateau (Qin et al., 2022), and in the Gobi of Inner Mongolia (Han et al., 2020). However, in the PMIP4 ensembles, the simulated MH GPP in China is 0.4 PgC lower than the PI condition (median of nine models) (Figure 2 and Figure S6 in Supporting Information S1). This mismatch is not surprising because the PMIP MH experiments only considered orbital forcing and greenhouse gases, while other boundary conditions (e.g., vegetation cover, ice sheets, and aerosols) were set the same as the PI period. This is due to the lack of a comprehensive and reliable global data set of vegetation for the MH (Otto-Bliesner et al., 2017). PMIP MH experiments simulated carbon cycle with static vegetation cover (Brierley et al., 2020), therefore the GPP in China is expected to be underestimated. Our model forced with GCM climatology and PIV (i.e., the MH_GCM_PIV experiment) also produces a 0.4 PgC lower GPP in the MH than

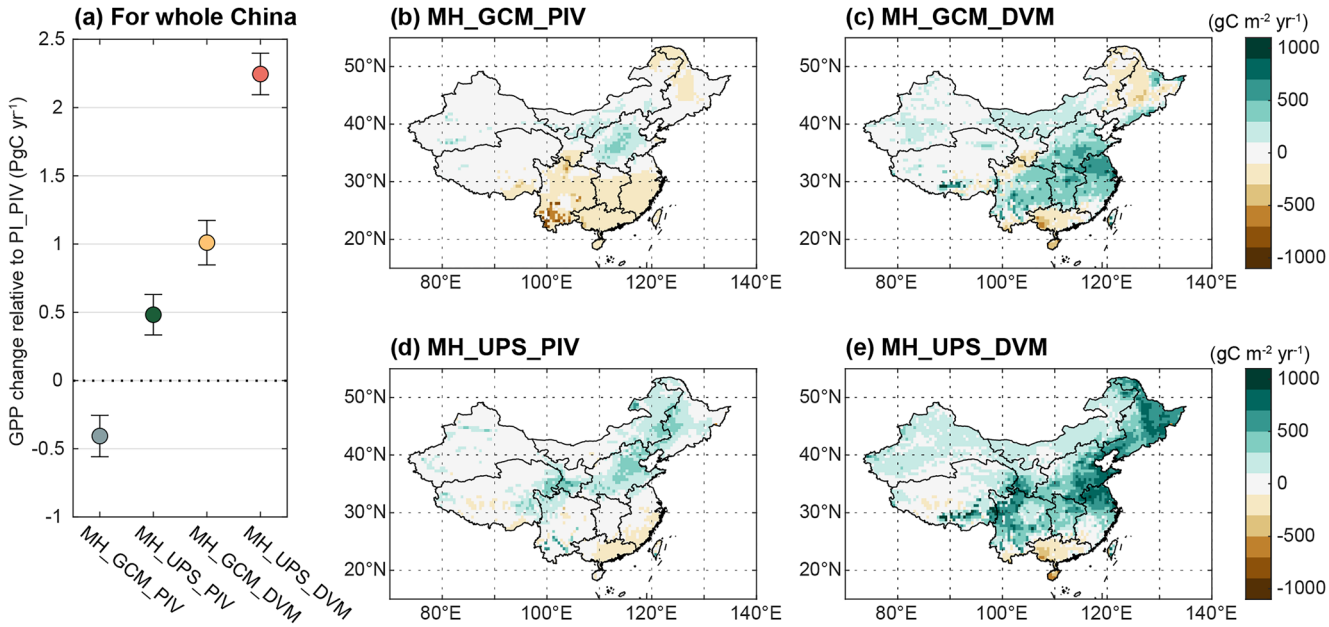

Figure 3. Changes in gross primary productivity (GPP) as a result of climate and land cover changes during the mid-Holocene (MH) in China, relative to the pre-industrial period (PI_PIV simulation). GCM and UPS represent climate forcing derived from a general circulation model and upscaled climate data, respectively. Land cover is either prescribed as PIV or simulated with DVM (see main text for details).

the PI. The simulated GPP in China increases by ∼1.0 PgC when using improved warmer and wetter MH climate forcing from Chen, Xiao, et al. (2022). Equally, considering the changes in vegetation types by activating DVM can further increase the GPP by ∼1.6 PgC. As a result, our improved estimates suggest that the MH GPP of ∼7.5 PgC/yr in China is higher than the PI period and the present day owing to more favorable climate conditions (Shi et al., 2021) and less anthropogenic land use (Goldewijk et al., 2017) during the MH (Figure 3). This work highlights the importance of incorporating vegetation dynamics in land surface modeling to correctly simulate the terrestrial carbon cycle in the past, since this may be the primary factor influencing vegetation GPP reconstructions. Likewise, reliable climate data are required for accurately simulating vegetation dynamics in MH China.

4.2. Potential Vegetation Biophysical Feedbacks on Climate

Many transient experiments suggest a cooler climate in the MH compared to PI—in contrast to paleoclimate records (Osman et al., 2021). This issue is known as the Holocene temperature conundrum (Dong et al., 2022; Liu et al., 2014; Zhang et al., 2022). For example, PMIP4 MH climate simulations with prescribed PI vegetation cover produce a global cooling of −0.3°C relative to the PI simulation (Brierley et al., 2020). Some recent climate simulations that include realistic vegetation or DVM can reproduce a warmer MH climate (Chen, Zhang, et al., 2022; Thompson et al., 2022). Theoretically, vegetation biophysical feedbacks are largely controlled by LAI, a variable that affects climate by altering albedo, air emissivity, aerodynamic resistance, evapotranspiration and clouds (Zeng et al., 2017). As PMIP4 MH climate is wetter but cooler than PI climate in China, the beneficial effect of climate changes on LAI is underestimated under GCM forcing (Figure 4 and Figure S7 in Supporting Information S1). In contrast, the MH_UPS_DVM simulation produces LAI increases in most regions in China (especially in Northeast China, North China, and northern Southeast China) relative to the PI_PIV experiment (Figure 4), consistent with changes in landscape openness inferred from palynological data (Li et al., 2019). Since trees generally have lower albedo than grasses and deserts, the increased LAI and tree cover significantly reduced albedo and consequently caused more absorbed radiation at the land surface (Figure 4 and Figure S8 in Supporting Information S1). Besides, the greenhouse effect of atmospheric water vapor due to more evapotranspiration may further result in warming feedback (Figure 4). In particular, increased tree cover alone during the MH led to an increase in surface net radiation, especially in northern China, which can heat the atmosphere through sensible heat flux (Figure S8 in Supporting Information S1). These processes have been shown to play an important role in explaining the high-latitude warming during the MH (Chen, Zhang, et al., 2022). In addition, increased LAI

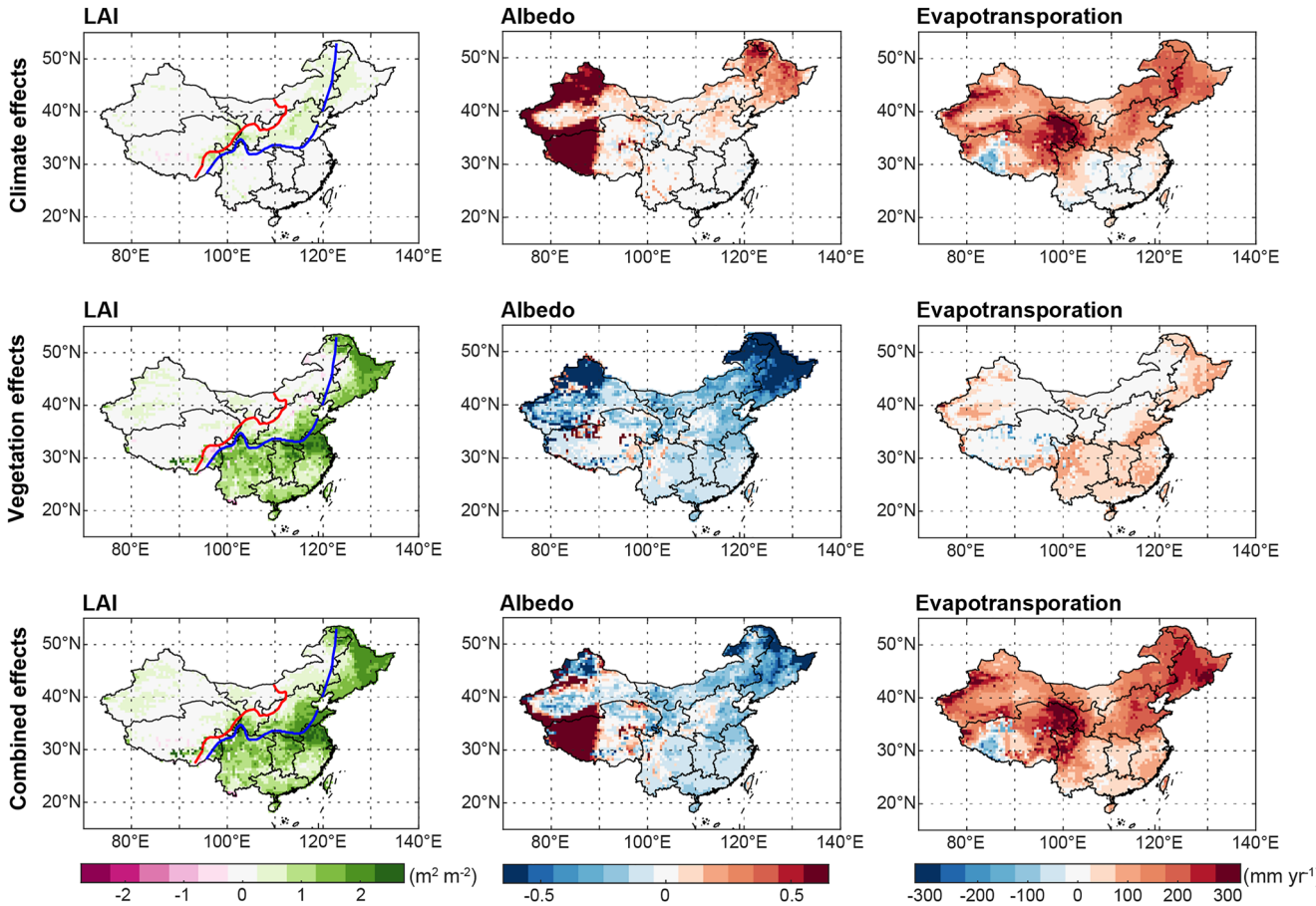

Figure 4. Terrestrial parameters of the mid-Holocene simulations relative to the pre-industrial period. Changes in mean annual leaf area index (LAI), albedo and evapotranspiration because of climate effects (i.e., MH_UPS_PIV–PI_PIV), vegetation effects (i.e., MH_UPS_DVM–MH_UPS_PIV) and combined effects (i.e., MH_UPS_DVM–PI_PIV). The blue and red lines represent the boundary between forest and steppe estimated from pollen data sets at 1 and 6 ka, respectively, simplified from Li et al. (2019).

may have an inter-seasonal impact and warm winters (Lian et al., 2022; Strandberg et al., 2022). For example, simulations using pollen-based vegetation in Europe showed 0–5°C warmer conditions in the MH than the PI, with the strongest warming in winter (Strandberg et al., 2022). Therefore, we suggest that the vegetation biophysical feedbacks can partially explain the mismatch between proxies and models in estimated temperature over China during the MH, especially the low winter temperature bias inherent in climate simulations (Lin et al., 2019; Zhang et al., 2022).

Regionally, the climate is also highly regulated by local land cover changes. In the central and western Qinghai-Tibet Plateau, more snowfall in the MH than the PI led to higher albedo resulting in lower temperatures and no increase in tree cover (Figure 4, Figures S1 and S8 in Supporting Information S1). This is in line with recent climate and vegetation reconstructions showing cooler climate and stable woody cover in this region during the MH (Cheng et al., 2022; Wang et al., 2021). In addition, recent PMIP4 ensembles can reproduce the enhanced precipitation of the MH, but the magnitude of this precipitation increase was still underestimated (Figure S1 in Supporting Information S1). Our results show that the enhanced vegetation growth is associated with more evapotranspiration (Figure 4 and Figure S7 in Supporting Information S1). It implies that the LAI-induced intensified water recycling may contribute to increased precipitation, thus helping to reconcile this discrepancy.

4.3. Uncertainties and Implications

This work forces a land surface model with improved climate fields for the MH and provide a high-resolution and spatially continuous gridded data of vegetation cover in China. Since the UPS forcing is produced with

pollen-based climate reconstructions (Chen, Xiao, et al., 2022; Lin et al., 2019) and half of the pollen data for evaluation of the simulated MH vegetation are also taken from Lin et al. (2019) (Figure 1), there are potential circularity. Thus, we further compared our simulation with the pollen-based quantitative Holocene plant cover at 69 grid cells (Figure S9; Text S1 in Supporting Information S1). Our simulation broadly captures the MH vegetation cover reconstructed by Li et al. (2023) in Qinghai-Tibet Plateau, Northwest China, and North China, except Northeast China, Central China and Southeast China (Figure S9 in Supporting Information S1). For these grids on average, our result overestimates coniferous and broadleaved trees by 9% and 6%, respectively (Figure S9 in Supporting Information S1). On the one hand, this is because grasses cannot grow under trees and trees tend to compete over grasses in our DVM. On the other hand, Li et al. (2023) declared that the pollen-based plant cover tends to overestimate open land due to the limitation of available pollen taxa. Besides the limitations of both methods, Li et al. (2023) considered anthropogenic land-cover change and therefore produced less woody cover while we simulated natural vegetation cover. Therefore, future attempts to improve the simulated vegetation cover may use a more realistic climate forcing, or combine land surface model and pollen-based vegetation reconstructions.

Previous coupled vegetation-atmosphere simulations have demonstrated that vegetation changes in the North Africa (Piao et al., 2020; Sun et al., 2019) and Northeast Asia (Chen et al., 2021) may impact the MH EASM through atmospheric and oceanic teleconnections. Li et al. (2022) explored the MH vegetation feedback on precipitation in northern China using climate simulations with dynamic vegetation. However, a reliable and spatially continuous land cover map is required to accurately include feedbacks from the forest expansion in China. With our vegetation map based on geological data sets and modeling techniques, this work reveals the impact of MH vegetation changes in China on terrestrial energy and hydrological budgets and potentially on climate, but cannot quantify the climate feedbacks since land-atmosphere interactions are also associated with other atmospheric processes and parameters (e.g., atmospheric circulation, atmospheric water vapor, clouds and downward radiation). Thus, we encourage an improved MH climate simulation by considering vegetation biophysical effects in China to better reconstruct the warm and wet climate.

5. Conclusions

Our simulations demonstrate that mid-Holocene gross primary productivity in China was higher than at present, benefiting from the warmer and wetter climate and less anthropogenic land use. Model ensembles in PMIP4 significantly underestimate mid-Holocene vegetation growth, primarily because the vegetation cover is prescribed using pre-industrial conditions, inconsistent with mid-Holocene palynological data. Enhanced vegetation growth during the mid-Holocene likely affects regional climate by altering terrestrial parameters, which have the potential to explain the previous model-data discrepancies in China. Taken together, our findings reveal the impact of vegetation cover on the terrestrial carbon cycle, and energy and hydrological budgets in China during the mid-Holocene. This work highlights the need to incorporate vegetation dynamics in terrestrial or climate simulations for the past and future.

Data Availability Statement

All information and data sets supporting the conclusions are available online. The simulation data to reproduce the figures and the results in this study are publicly available in Chen et al. (2023).

Acknowledgments
We appreciate CMIP6/PMIP4 groups, TRENDY groups, and Yitong Yao and Shilong Piao for sharing their simulated GPP data. We thank the BIOME6000 groups, and Yating Lin and Haibin Wu for making available their pollen compilations. This study was supported by the National Natural Science Foundation of China (Nos. 42230208 and 42307556), the Natural Science Foundation of Hubei Province (No. 2023AFB024), the China Postdoctoral Science Foundation (No. 2021M692976), and the Fundamental Research Funds for the Central Universities the China University of Geosciences (Wuhan) (No. CUG2106323). This work was performed using HPC resources from GENCI-TGCC (Grant 2022-A0130206328).

References

Anav, A., Friedlingstein, P., Beer, C., Ciais, P., Harper, A., Jones, C., et al. (2015). Spatiotemporal patterns of terrestrial gross primary production: A review. *Reviews of Geophysics*, *53*(3), 785–818. https://doi.org/10.1002/2015rg000483

Blyth, E. M., Arora, V. K., Clark, D. B., Dadson, S. J., De Kauwe, M. G., Lawrence, D. M., et al. (2021). Advances in land surface modelling. *Current Climate Change Reports*, *7*(2), 45–71. https://doi.org/10.1007/s40641-021-00171-5

Boucher, O., Servonnat, J., Albright, A. L., Aumont, O., Balkanski, Y., Bastrikov, V., et al. (2020). Presentation and evaluation of the IPSL-CM6A-LR climate model. *Journal of Advances in Modeling Earth Systems*, *12*(7), e2019MS002010. https://doi.org/10.1029/2019ms002010

Bova, S., Rosenthal, Y., Liu, Z., Godad, S. P., & Yan, M. (2021). Seasonal origin of the thermal maxima at the Holocene and the last interglacial. *Nature*, *589*(7843), 548–553. https://doi.org/10.1038/s41586-020-03155-x

Braconnot, P., Albani, S., Balkanski, Y., Cozic, A., Kageyama, M., Sima, A., et al. (2021). Impact of dust in PMIP-CMIP6 mid-Holocene simulations with the IPSL model. *Climate of the Past*, *17*(3), 1091–1117. https://doi.org/10.5194/cp-17-1091-2021

Brierley, C. M., Zhao, A. N., Harrison, S. P., Braconnot, P., Williams, C. J. R., Thornalley, D. J. R., et al. (2020). Large-scale features and evaluation of the PMIP4-CMIP6 midHolocene simulations. *Climate of the Past*, *16*(5), 1847–1872. https://doi.org/10.5194/cp-16-1847-2020

Chen, J., Zhang, Q., Huang, W., Lu, Z. Y., Zhang, Z. P., & Chen, F. H. (2021). Northwestward shift of the northern boundary of the East Asian summer monsoon during the mid-Holocene caused by orbital forcing and vegetation feedbacks. *Quaternary Science Reviews*, *268*, 107136. https://doi.org/10.1016/j.quascirev.2021.107136

Chen, J., Zhang, Q., Kjellström, E., Lu, Z., & Chen, F. (2022). The contribution of vegetation-climate feedback and resultant sea ice loss to amplified arctic warming during the mid-Holocene. *Geophysical Research Letters*, *49*(18), e2022GL098816. https://doi.org/10.1029/2022gl098816

Chen, W., Xiao, A., Braconnot, P., Ciais, P., Viovy, N., & Zhang, R. (2022). Mid-Holocene high-resolution temperature and precipitation gridded reconstructions over China: Implications for elevation-dependent temperature changes. *Earth and Planetary Science Letters*, *593*, 117656. https://doi.org/10.1016/j.epsl.2022.117656

Chen, W., Zhang, Z., Ciais, P., Tan, L., Kemp, D., & Viovy, N. (2023). Enhanced mid-Holocene vegetation growth and its biophysical feedbacks in China (Version 2) [Dataset]. Mendeley Data. https://doi.org/10.17632/4vfmsb54d6

Chen, W. Z., Ciais, P., Zhu, D., Ducharne, A., Viovy, N., Qiu, C. J., & Huang, C. (2020). Feedbacks of soil properties on vegetation during the Green Sahara period. *Quaternary Science Reviews*, *240*, 106389. https://doi.org/10.1016/j.quascirev.2020.106389

Cheng, Y., Liu, H. Y., Han, Y., & Hao, Q. (2022). Climate sustained the evolution of a stable postglacial woody cover over the Tibetan Plateau. *Global and Planetary Change*, *215*, 103880. https://doi.org/10.1016/j.gloplacha.2022.103880

Dallmeyer, A., Claussen, M., & Brovkin, V. (2019). Harmonising plant functional type distributions for evaluating Earth system models. *Climate of the Past*, *15*(1), 335–366. https://doi.org/10.5194/cp-15-335-2019

Dong, Y., Wu, N., Li, F., Zhang, D., Zhang, Y., Shen, C., & Lu, H. (2022). The Holocene temperature conundrum answered by mollusk records from East Asia. *Nature Communications*, *13*(1), 5153. https://doi.org/10.1038/s41467-022-32506-7

Gao, G. Z., Rand, E., Li, N. N., Li, D. H., Wang, J. Y., Niu, H. H., et al. (2022). East Asian monsoon modulated Holocene spatial and temporal migration of forest-grassland ecotone in Northeast China. *CATENA*, *213*, 106151. https://doi.org/10.1016/j.catena.2022.106151

Goldewijk, K. K., Beusen, A., Doelman, J., & Stehfest, E. (2017). Anthropogenic land use estimates for the Holocene - HYDE 3.2. *Earth System Science Data*, *9*(2), 927–953. https://doi.org/10.5194/essd-9-927-2017

Goldsmith, Y., Broecker, W. S., Xu, H., Polissar, P. J., de Menocal, P. B., Porat, N., et al. (2017). Northward extent of East Asian monsoon covaries with intensity on orbital and millennial timescales. *Proceedings of the National Academy of Sciences of the United States of America*, *114*(8), 1817–1821. https://doi.org/10.1073/pnas.1616708114

Guimberteau, M., Zhu, D., Maignan, F., Huang, Y., Yue, C., Dantec-Nedelec, S., et al. (2018). ORCHIDEE-MICT (v8.4.1), a land surface model for the high latitudes: Model description and validation. *Geoscientific Model Development*, *11*(1), 121–163. https://doi.org/10.5194/gmd-11-121-2018

Han, Y., Liu, H. Y., Zhou, L. Y., Hao, Q., & Cheng, Y. (2020). Postglacial evolution of forest and grassland in southeastern Gobi (Northern China). *Quaternary Science Reviews*, *248*, 106611. https://doi.org/10.1016/j.quascirev.2020.106611

Harrison (2017). BIOME 6000 DB classified plotfile version 1. Retrieved from: http://researchdata.reading.ac.uk/99/

He, Y., Dong, W., Ji, J., & Dan, L. (2005). The terrestrial NPP simulation in China since 6ka BP. *Journal of Meteorological Research*, *19*(4), 492–500.

Jiang, D. B., Lang, X. M., Tian, Z. P., & Wang, T. (2012). Considerable model-data mismatch in temperature over China during the mid-Holocene: Results of PMIP simulations. *Journal of Climate*, *25*(12), 4135–4153. https://doi.org/10.1175/jcli-d-11-00231.1

Kaufman, D. S., & Broadman, E. (2023). Revisiting the Holocene global temperature conundrum. *Nature*, *614*(7948), 425–435. https://doi.org/10.1038/s41586-022-05536-w

Krinner, G., Viovy, N., de Noblet-Ducoudré, N., Ogée, J., Polcher, J., Friedlingstein, P., et al. (2005). A dynamic global vegetation model for studies of the coupled atmosphere-biosphere system. *Global Biogeochemical Cycles*, *19*(1), GB1015. https://doi.org/10.1029/2003GB002199

Le Quéré, C., Andrew, R. M., Friedlingstein, P., Sitch, S., Pongratz, J., Manning, A. C., et al. (2018). Global carbon budget 2017. *Earth System Science Data*, *10*(1), 405–448. https://doi.org/10.5194/essd-10-405-2018

Li, F., Gaillard, M.-J., Cao, X., Herzschuh, U., Sugita, S., Ni, J., et al. (2023). Gridded pollen-based Holocene regional plant cover in temperate and northern subtropical China suitable for climate modelling. *Earth System Science Data*, *15*(1), 95–112. https://doi.org/10.5194/essd-15-95-2023

Li, Q., Wu, H. B., Yu, Y. Y., Sun, A. Z., & Luo, Y. L. (2019). Large-scale vegetation history in China and its response to climate change since the Last Glacial Maximum. *Quaternary International*, *500*, 108–119. https://doi.org/10.1016/j.quaint.2018.11.016

Li, X. Z., Liu, X. D., Pan, Z. T., Xie, X. N., Shi, Z. G., Wang, Z. S., & Bai, A. (2022). Orbital-scale dynamic vegetation feedback caused the Holocene precipitation decline in northern China. *Communications Earth & Environment*, *3*(1), 257. https://doi.org/10.1038/s43247-022-00596-2

Lian, X., Jeong, S., Park, C. E., Xu, H., Li, L. Z. X., Wang, T., et al. (2022). Biophysical impacts of northern vegetation changes on seasonal warming patterns. *Nature Communications*, *13*(1), 3925. https://doi.org/10.1038/s41467-022-31671-z

Lin, Y. T., Ramstein, G., Wu, H. B., Rani, R., Braconnot, P., Kageyama, M., et al. (2019). Mid-Holocene climate change over China: Model-data discrepancy. *Climate of the Past*, *15*(4), 1223–1249. https://doi.org/10.5194/cp-15-1223-2019

Liu, Z., Zhu, J., Rosenthal, Y., Zhang, X., Otto-Bliesner, B. L., Timmermann, A., et al. (2014). The Holocene temperature conundrum. *Proceedings of the National Academy of Sciences of the United States of America*, *111*(34), E3501–E3505. https://doi.org/10.1073/pnas.1407229111

Martin Calvo, M., & Prentice, I. C. (2015). Effects of fire and CO2 on biogeography and primary production in glacial and modern climates. *New Phytologist*, *208*(3), 987–994. https://doi.org/10.1111/nph.13485

O'ishi, R., & Abe-Ouchi, A. (2013). Influence of dynamic vegetation on climate change and terrestrial carbon storage in the Last Glacial Maximum. *Climate of the Past*, *9*(4), 1571–1587. https://doi.org/10.5194/cp-9-1571-2013

Osman, M. B., Tierney, J. E., Zhu, J., Tardif, R., Hakim, G. J., King, J., & Poulsen, C. J. (2021). Globally resolved surface temperatures since the Last Glacial Maximum. *Nature*, *599*(7884), 239–244. https://doi.org/10.1038/s41586-021-03984-4

Otto-Bliesner, B. L., Braconnot, P., Harrison, S. P., Lunt, D. J., Abe-Ouchi, A., Albani, S., et al. (2017). The PMIP4 contribution to CMIP6-Part 2: Two interglacials, scientific objective and experimental design for Holocene and Last Interglacial simulations. *Geoscientific Model Development*, *10*(11), 3979–4003. https://doi.org/10.5194/gmd-10-3979-2017

Piao, J. L., Chen, W., Wang, L., Pausata, F. S. R., & Zhang, Q. (2020). Northward extension of the East Asian summer monsoon during the mid-Holocene. *Global and Planetary Change*, *184*, 103046. https://doi.org/10.1016/j.gloplacha.2019.103046

Prentice, I. C., Harrison, S. P., & Bartlein, P. J. (2011). Global vegetation and terrestrial carbon cycle changes after the last ice age. *New Phytologist*, *189*(4), 988–998. https://doi.org/10.1111/j.1469-8137.2010.03620.x

Qin, F., Zhao, Y., & Cao, X. Y. (2022). Biome reconstruction on the Tibetan Plateau since the Last Glacial Maximum using a machine learning method. *Science China Earth Sciences*, *65*(3), 518–535. https://doi.org/10.1007/s11430-021-9867-1

Shi, F., Lu, H. Y., Guo, Z. T., Yin, Q. Z., Wu, H. B., Xu, C. X., et al. (2021). The position of the current warm period in the context of the past 22,000 years of summer climate in China. *Geophysical Research Letters*, *48*(5), e2020GL091940. https://doi.org/10.1029/2020gl091940

Strandberg, G., Lindstrom, J., Poska, A., Zhang, Q., Fyfe, R., Githumbi, E., et al. (2022). Mid-Holocene European climate revisited: New high-resolution regional climate model simulations using pollen-based land-cover. *Quaternary Science Reviews*, *281*, 107431. https://doi.org/10.1016/j.quascirev.2022.107431

Sun, W. Y., Wang, B., Zhang, Q., Pausata, F. S. R., Chen, D. L., Lu, G. N., et al. (2019). Northern hemisphere land monsoon precipitation increased by the green Sahara during middle Holocene. *Geophysical Research Letters*, *46*(16), 9870–9879. https://doi.org/10.1029/2019gl082116

Thompson, A. J., Zhu, J., Poulsen, C. J., Tierney, J. E., & Skinner, C. B. (2022). Northern Hemisphere vegetation change drives a Holocene thermal maximum. *Science Advances*, *8*(15), eabj6535. https://doi.org/10.1126/sciadv.abj6535

Wang, M. D., Hou, J. Z., Duan, Y. W., Chen, J. H., Li, X. M., He, Y., et al. (2021). Internal feedbacks forced middle Holocene cooling on the Qinghai-Tibetan Plateau. *Boreas*, *50*(4), 1116–1130. https://doi.org/10.1111/bor.12531

Wei, Y., Liu, S., Huntzinger, D. N., Michalak, A. M., Viovy, N., Post, W. M., et al. (2014). The north American carbon program multi-scale synthesis and terrestrial model intercomparison project - Part 2: Environmental driver data. *Geoscientific Model Development*, *7*(6), 2875–2893. https://doi.org/10.5194/gmd-7-2875-2014

Wu, B. L., Lang, X. M., & Jiang, D. B. (2021). Migration of the northern boundary of the east Asian summer monsoon over the last 21,000 years. *Journal of Geophysical Research: Atmospheres*, *126*(17), e2021JD035078. https://doi.org/10.1029/2021jd035078

Yang, B., Qin, C., Brauning, A., Osborn, T. J., Trouet, V., Ljungqvist, F. C., et al. (2021). Long-term decrease in Asian monsoon rainfall and abrupt climate change events over the past 6,700 years. *Proceedings of the National Academy of Sciences of the United States of America*, *118*(30), e2102007118. https://doi.org/10.1073/pnas.2102007118

Yao, Y., Wang, X., Li, Y., Wang, T., Shen, M., Du, M., et al. (2018). Spatiotemporal pattern of gross primary productivity and its covariation with climate in China over the last thirty years. *Global Change Biology*, *24*(1), 184–196. https://doi.org/10.1111/gcb.13830

Zeng, Z. Z., Piao, S. L., Li, L. Z. X., Zhou, L. M., Ciais, P., Wang, T., et al. (2017). Climate mitigation from vegetation biophysical feedbacks during the past three decades. *Nature Climate Change*, *7*(6), 432–436. https://doi.org/10.1038/nclimate3299

Zhang, W., Wu, H., Cheng, J., Geng, J., Li, Q., Sun, Y., et al. (2022). Holocene seasonal temperature evolution and spatial variability over the Northern Hemisphere landmass. *Nature Communications*, *13*(1), 5334. https://doi.org/10.1038/s41467-022-33107-0

Zhang, Y., Marquer, L., Cui, Q. Y., Zheng, Z., Zhao, Y., Wan, Q. C., & Zhou, A. (2021). Holocene vegetation changes in the transition zone between subtropical and temperate ecosystems in Eastern Central China. *Quaternary Science Reviews*, *253*, 106768. https://doi.org/10.1016/j.quascirev.2020.106768

Zhou, X., Zhan, T., Tu, L., Smol, J. P., Jiang, S., Liu, X., et al. (2021). Monthly insolation linked to the time-transgressive nature of the Holocene East Asian monsoon precipitation maximum. *Geology*, *50*(3), 331–335. https://doi.org/10.1130/g49550.1

Zhu, D., Ciais, P., Chang, J., Krinner, G., Peng, S., Viovy, N., et al. (2018). The large mean body size of mammalian herbivores explains the productivity paradox during the Last Glacial Maximum. *Nature Ecology & Evolution*, *2*(4), 640–649. https://doi.org/10.1038/s41559-018-0481-y